Journal of Cleaner Production 390 (2023) 136098

Contents lists available at ScienceDirect

Journal of Cleaner Production

journal homepage: www.elsevier.com/locate/jclepro

Characterization of sustainable building materials obtained from textile waste: From laboratory prototypes to real-world manufacturing processes

Chiara Rubino *, Stefania Liuzzi, Pietro Stefanizzi, Francesco Martellotta

[a] Dipartimento di Architettura, Costruzione e Design, Politecnico di Bari, via Orabona 4, I-70125, Bari, Italy

ARTICLE INFO

Handling Editor: Cecilia Maria Villas Bôas de Almeida

Keywords:
Textile waste
Raw materials substitution
Waste reduction
Sustainable building
Energy efficiency
Sound insulation

ABSTRACT

The limited availability of natural resources and the environmental impacts related to their extraction are the main reasons for developing construction materials using industrial residues as raw materials. On the other hand, the growing attention to the well-being of building occupants encourages the scientific community in proposing strategies not only sustainable, but also able to improve both the indoor acoustic and thermal comfort. The present work proposes nonwoven materials differing in density and thickness, obtained from textile waste, following an airlaying industrial process. The acoustic and thermal performances of the developed materials were investigated. Air flow resistivity was lower than 100 kN s/m^4 resulting in diffuse sound absorption coefficients higher than 0.6 starting from 500 Hz for 2.5 cm thick panels. A detailed characterization of the damping properties of the prepared samples (i.e. a total dynamic stiffness ranging from 7 to 13 MN/m^3 and an average loss factor ranging from 0.22 to 0.27), made it possible to model the sound insulation behaviour, proving significant improvements when the materials were applied as resilient layers in a floating floor or as insulating material in opaque façades. Furthermore, all the tested nonwovens showed a thermal conductivity lower than 0.05 W/(m·K), representing a good solution for the improvement of the energy efficiency of the building envelope.

1. Introduction

Improving thermal efficiency of the building envelope has become an important target to deal as early as 2002, when the European Commission first tried to limit the negative impacts of buildings sector on climate change, promoting the reduction of carbon and greenhouse gas emissions (Directive 2002/91/EC, 2002). Energy renovation measures not only lead to a reduction of energy demand by minimizing the heat transmission during the cooling and heating of the building, but should also have positive effects on the indoor thermal comfort preserving the health and wellbeing of the occupants. However, recent research (Khan and Bhattacharjee, 2021; Kaushik et al., 2020) highlighted the need to combine thermal and acoustic conditions for reaching a global comfortable indoor environment. In fact, the rapid industrialization and urbanization of the cities in the last years emphasized noise pollution issues which are becoming more and more pervasive leading to the introduction of strict legislative constraints to control noise and vibrations in buildings (Ji et al., 2019).

The environmental impacts of buildings in terms of intensive use of non-renewable resources, waste generation, dust and gas emissions, fueled a global challenge in the construction industry to "become green". One way to achieve green building is to use more resource-efficient processes at every stage, including construction, renovation, operation, maintenance, and demolition, in order to save natural resources and to reduce the adverse environmental effects of their extraction. Therefore, waste management based on the recovery of resources became an important sub-sector of Circular Economy (Lu et al., 2019).

Recently, the European Commission introduced the European Green Deal (Directorate-General for Communication, 2020), a strategic policy aimed at mobilizing the building industry to reduce the intensive extraction of virgin resources by ensuring the use of the largest possible amount of secondary raw materials for the construction and renovation of buildings (Antolinc and Eleršic Filipic, 2021). An enormous literature framework in terms of sustainable building materials is now available. Several authors presented research studies about sustainable panels, made with recycled components, taken from biomasses and urban waste, with high thermal and noise insulation performances. Natural residues, derived from pruning waste or food industry represent a

* Corresponding author.
E-mail addresses: chiara.rubino@poliba.it (C. Rubino), stefania.liuzzi@poliba.it (S. Liuzzi), pietro.stefanizzi@poliba.it (P. Stefanizzi), francesco.martellotta@poliba.it (F. Martellotta).

https://doi.org/10.1016/j.jclepro.2023.136098
Received 25 July 2022; Received in revised form 20 December 2022; Accepted 16 January 2023
Available online 20 January 2023

Nomenclature

c_p	specific heat capacity J/(kg·K)
c	compressibility mm
d	thickness cm
d_L	thickness under a load of 250 Pa mm
d_F	thickness under a load of 2 kPa mm
d_B	thickness under a load of 50 kPa mm
f_r	resonant frequency Hz
$h(c)$	percentage thickness decrease %
κ	internal areal heat capacity kJ/(m^2·K)
$k_0^{'}$	static thermal permeability m^2
s'	dynamic stiffness per unit of area N/m^3
s_a'	dynamic stiffness of air N/m^3
s_t'	apparent dynamic stiffness per unit of area N/m^3
C	spectrum adaptation term (pink noise) dB
C_{tr}	spectrum adaptation term (road traffic noise) dB
D	thermal diffusivity m^2/s
E	modulus of elasticity N/m^2
L_n	impact sound pressure level dB
$L_{n,w}$	normalized weighted sound pressure level dB
M_S	surface mass kg/m^2
R_w	weighted sound transmission index dB
TL	transmission loss dB
T_{30}	reverberation time s
U	thermal transmittance W/(m^2·K)
V	volume m^3
Y_{mn}	periodic thermal transmittance W/(m^2·K)
$\alpha\perp$	normal incidence sound absorption coefficient
α_{sab}	random incidence sound absorption coefficient
ε	open porosity
η	loss factor
λ	thermal conductivity W/(m·K)
υ	Poisson's ratio
ρ	density kg/m^3
ρc	volumetric heat capacity J/(m^3·K)
σ	air flow resistivity kN·s/m^4
σ_s	air flow resistance kN·s/m^3
Δt	time shift h

Subscripts

bulk	bulk value including open pores
true	true value excluding open pores

serious issue in terms of disposal. Nevertheless, this kind of materials proved to be very useful if used in combination with other materials, to create new construction processes. Different types of natural aggregates like hemp (Liao et al., 2020), straw (Czajkowski et al., 2022), almond skins (Liuzzi et al., 2020), rice husk (Taban et al., 2019), palm (Belakroum et al., 2017), olive waste (Martellotta et al., 2018) or sugarcane bagasse (Mehrzad et al., 2022) have been tested by the scientific community. Among the bio-based raw materials, cork (Trematerra and Lombardi, 2017), sheep wool (ZachKorjenic et al., 2012), jute (Samanta et al., 2021) and kenaf (Berardi and Iannace, 2015) also received large attention during the last decade as sustainable alternative to synthetic components for building materials.

Considering urban waste, textile fibers derived from industrial manufacturing process are playing an increasing role as secondary raw resources, particularly because their ability to enhance the porosity of building materials that may improve both thermal and acoustic properties. Lacoste et al. (2018) developed composite materials based on wood fibers and textile waste which could be considered good eco-insulators, exhibiting a thermal conductivity varying from 0.078 to 0.089 W/(m·K) with a density in the range of 308–333 kg/m^3. Binici et al. (2014) used plaster or epoxy as binders to mix agricultural and textile waste previously grinded. The obtained boards were applied to walls of a test room and an improvement of the sound insulation performances of the walls was proved. Sakthivel et al. (2021) proposed recycled cotton/polyester nonwovens with excellent sound absorption ability especially in the high frequency range above 2000 Hz.

Furthermore, apparel waste textiles are usually obtained by combining materials of natural origin (i.e. cotton, linen, wool) and synthetic ones (usually polyester) needing greater efforts to be recycled (Briga-Sá et al., 2013). The conversion of textile waste into secondary raw materials is all the more essential considering that in 2030 textile waste in the world will be 17.5 kg per capita (Kamble and Behera, 2021).

An important acoustic ability of a porous material, in addition to acoustic insulation, is the sound absorption capacity. It may be mostly influenced by the structure of the pores, which also depends from the manufacturing process and the raw materials used for the production of the building component (Karimi et al., 2022). For example, taking into account the properties of the fibrous materials it is fundamental to assess the physical properties as fineness, length and cross-section; these performances could assume a really important role in influencing the sound absorption performance of the final product (Atiénzar-Navarro et al., 2022). On the other side, fibrous sound absorbers have been largely widespread also due to their good thermal insulation properties related to their microstructure consisted in a complex pattern of fibers and air (Ghermezgoli et al., 2021).

In a previously published work (Rubino et al., 2021), the authors already investigated the potential of textile waste in association with different binders. One of the most promising (later on referred as "BICO") was made from textile waste fibers and bicomponent fibers as binder. The results showed that the manufacturing process affected pore microstructure of the final products, with consequence especially on the sound absorption and water vapour diffusion properties. However, all tested samples exhibited good thermal and acoustic performances to replace conventional building materials.

Based on the above mentioned promising results, the present work aims at completing the preliminary research by analyzing materials resulting from the industrial scale-up of the most promising combinations previously investigated. Nonwovens materials obtained from textile waste and bicomponent fibers as binder were produced by an airlaying industrial production process. A detailed characterization of the resulting materials was carried out in the laboratory. Sound absorption curves were experimentally determined both under normal and random incidence conditions. The obtained curves were discussed with reference to the phenomenological theoretical models and the required non-acoustical properties were determined. Furthermore, thermal insulation performance was evaluated through the measurement of the thermal conductivity and the elastic and damping properties were experimentally investigated. The results of the laboratory tests were then compared with those previously published obtained from preliminary laboratory samples (Rubino et al., 2021), in order to demonstrate the effectiveness of the industrial production processes in achieving the expected acoustic and thermal properties. Lastly, the possibility of using the studied materials in combination with existing building structures to improve their noise control behavior was explored by computing their acoustic behaviour by means of the *Alpha*Cell® software, starting from the measured acoustic and damping properties. The thermal measured properties were instead useful to evaluate the effect of adding the tested materials on the thermal insulating performance of building envelope, according to ISO 13786 (2008).

2. Materials and methods

2.1. Material fabrication

Textile wastes were used as base fibers for producing different nonwoven materials for building applications. An industrial airlaying process was followed, using the Copolyester/polyester (Co PET/PET) sheath-core bi-component fibers as thermally bondable fibers. The raw materials used in this work (i.e. the textile base and the synthetic binder fibers) belonged to the same batches considered to produce the BICO samples at laboratory scale. Therefore, they were widely characterized in the previously published work (Rubino et al., 2021), where their thermal behaviour was particularly investigated by means of a Differential Scanning Calorimeter (DSC) analysis, in order to choose the suitable working temperature able to avoid the decay of the natural polymer and to ensure the binding action of the synthetic one. For the sake of brevity, the most important properties of the raw materials are reported below, while details could be found in Rubino et al. (2021).

To minimize transportation costs, textile wastes were supplied by the local company Gordon Confezioni srl and were selected among tailoring of the autumn-winter collection, resulting mainly made of wool. The analysis of the diameter distribution of the wool fibers showed values ranging from 8 to 34 μm, with a mean value of 19 μm and a standard deviation of 7 μm. The results of the DSC analysis showed that the decomposition of the wool, with the consequent breakdown of the chemical bonds, started from about 250 °C. Copolyester/polyester (Co PET/PET) sheath-core bi-component fibers of 22 μm diameter were used as a binder. The main feature of this synthetic fiber relies in the two different polymers used, having melting temperatures (obtained from the DSC analysis), of 70 °C for the copolyester polymer and 253 °C for the polyester.

The textile wastes shown in Fig. 1(a) consisted not only in yarns, but also in fabric remnants. They were first subjected to a "rag grinding" process able to transform them by first cutting and then tearing pieces. Wastes longer than about 50 mm needed to be further cut before the grinding process which returned the material in the state shown in Fig. 1 (b). The conversion of wastes into building panels was obtained by blending textile fibers with Copolyester/polyester (Co PET/PET) sheath-core bi-component fibers used as binder. As it can be observed in Fig. 2, the bi-component fibers and the textile waste batt were uniformly dispersed in an airstream with the aim to obtain a mix of fibers which did not interact each other mechanically or by friction. This fibers mixture was led towards a permeable conveyor where they were randomly deposited in the form of a web. The last step involved molding the web in an oven and then cutting it into panels. During heating, the bi-component fibers played a fundamental role: the copolyester worked as low melting polymer and softened to form the bond; while the polyester worked as higher melting polymer contributing to the structural integrity of the web. Therefore, the use of a bi-component fiber allowed to reduce the working temperature to 100 °C in order to combine the behaviors of the two synthetic polymers, while avoiding side effects on the natural fiber.

The percentage content of binder fibers was selected on the basis of previous investigations (Rubino et al., 2021) aimed at obtaining material properties comparable with those developed at laboratory scale. However, compared to those percentages, a 5% reduction was applied in this work. In fact, on one side the industrial process ensured increased homogeneity of the mixes compared to the laboratory process and this resulted in the need of a lower amount of binder. On the other hand, the laboratory samples were obtained starting from a 100% merino wool waste, while in this case, (given the larger amount needed), the waste materials employed also included a small fraction (nearly impossible to calculate accurately) of other synthetic fibers, which suggested to reduce by 5% the original fraction.

The final panels are shown in Fig. 3. As outlined in Table 1, three different types of textile waste nonwoven materials with different values of bulk density ρ_{bulk} and thickness d were manufactured (later on identified with the acronym TW followed by the numerical value of the density to identify the different samples). The values of density were chosen in order to be as close as possible to those of the prototypes previously developed at laboratory scale. The aim was to allow the comparison between the performances of the TW and BICO samples, proving that an industrial up-scaling was possible, while keeping the properties of the two materials unchanged. The different density values of the panels were obtained by varying the amount per square meter of textile fibers introduced in the production line, as a function of the expected panels thickness. The bi-component fiber was then added based on the amount of textile waste, keeping its percentage unvaried and equal to 15%. The values of ρ_{bulk} and d values reported in Table 1 are given as mean value with its measurement uncertainty expressed as the standard deviation of the mean, according to ISO/IEC Guide 98-3 (2008).

The acoustic and thermal properties of TW panels were analyzed by collecting experimental data and comparing them with data collected for BICO samples, in order to evaluate the effects of the manufacturing process as well as the effects related to the larger sample dimension.

2.2. Experimental measurement set-up

2.2.1. Morphological properties

Morphological analysis of the tested materials was carried out using a Scanning Electron Microscope (SEM) ZEISS, model ULTRA 55. The samples were prepared by cutting small slices from the larger panels and arranging them onto a double-sided adhesive carbon tab attached to an aluminum stub. All fractured surfaces were sputter-coated with gold prior to testing.

2.2.2. Non-acoustic properties

A direct characterization of the open porosity ε was performed using a ULTRAPYC 1200-e Quantachrome Helium gas Pycnometer. The experimental test was based on the measurement of the pressure drop occurred when a helium pressurized cell containing a cylindrical sample (3 cm diameter) was connected to a second empty cell of fixed volume. The true volume V_{true} (solid matter and closed pores) of the tested samples was obtained by exploiting the ideal gas behaviour of the helium. The true density value ρ_{true} of each material was calculated from

(a) (b) (c) (d)

Fig. 1. Raw materials: textile batts and bi-component fibers (a), mix of base and binder materials (b), fibers deposited in form of web before (c) and after (d) their treatment in the oven.

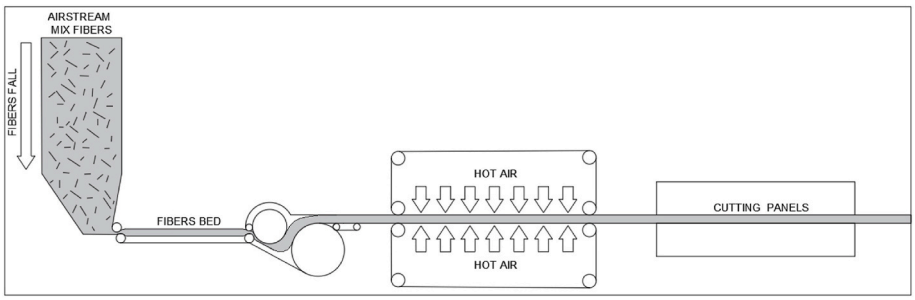

Fig. 2. Schematic diagram showing the airlaying process followed to form nonwoven TW panels.

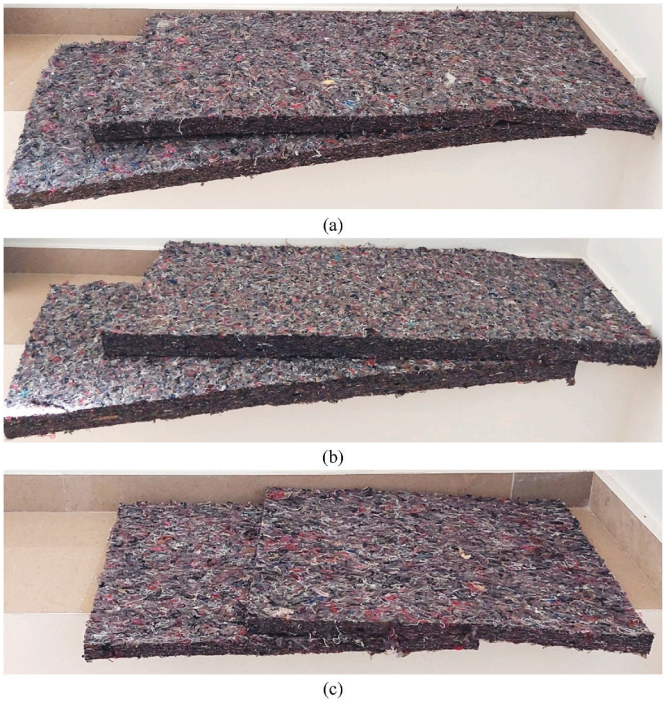

Fig. 3. Photographs of the samples of industrial production of TW-68 (a), TW-96 (b), and TW-134 (c) materials.

Table 1
Details of tested materials: bulk density values ρ_{bulk} and thickness values d (with measurement uncertainty expressed as standard deviation of the mean (ISO/IEC Guide 98-3, 2008)), number of panels n produced and area A of each panel.

Sample ID	ρ_{bulk} [kg/m^3]	d [cm]	A [cm^2]	n [-]
TW-68	68 ± 1.5	4.0 ± 0.08	120 × 60	8
TW-96	96 ± 4.5	5.1 ± 0.07	120 × 60	8
TW-134	134 ± 2.0	2.5 ± 0.03	60 × 60	16

the ratio between the mass of the tested samples and the true volume value provided by the pycnometer. The data obtained for each material were averaged over five measurements carried out on one sample for each type of material.

The air flow resistance σ_s of the tested materials was experimentally evaluated following the Ingard and Dear method (Ingard and Dear, 1985) measuring the difference in sound pressure created across the absorbent test material as a consequence of a sound field. The measurement setup consisted of a 5 mm thick methacrylate tube, with a 4 cm inner diameter, closed with a rigid termination at one end and with a 5 cm loudspeaker (Visaton FRS 5) with a frequency response spanning from 150 Hz to 20 kHz at the other end. The tube was made of two parts, 85 cm long each, between which the sample was inserted. Three samples for each type of material were tested. A pair of microphones (Core Sound) were located in front of the absorbent material and close to the rigid termination for measuring the pressure values of the sound field created using an exponential sine sweep of 10 s from 50 to 1000 Hz. The airflow resistance was calculated from the minima value of the modulus of the imaginary part of the transfer function between the microphone signals and extrapolating towards a zero frequency value. All processing was performed by a custom-made MATLAB® graphic user interface. The air flow resistance per unit layer thickness (i.e. the air flow resistivity σ) was finally calculated. Three samples for each type of material were tested.

2.2.3. Sound absorption properties

The normal incidence sound absorption coefficients $\alpha_\perp$ were directly determined according to standard ISO 10534-2 (1998), following the transfer-function method. A BSWA SW 260 impedance tube was used. A 20 W loudspeaker placed at one end of the tube produced acoustic plane waves on the front surface of the test sample placed at the opposite rigid end of the tube. Two ¼'' microphones mounted on the tube wall measured the pressure at two fixed positions, allowing to compute the complex transfer function between the measured signals. From this information and the distance between the microphones and the sample surface, it was possible to find the normal incidence reflection factor and, then, the normal incidence sound absorption curve. Two different tube configurations (with 60 and 30 mm inner diameter) were used in order to cover the frequency range from 100 to 6300 Hz. The 60 mm tube was characterized by a distance between the first microphone and the sample surface of 30 mm and by two different microphones spacing of 170 mm and 45.5 mm, resulting in a frequency range of 100 ÷ 630 Hz and 500 ÷ 2500 Hz, respectively. The tube with 30 mm inner diameter was characterized by a distance between the first microphone and surface sample of 30 mm and a microphones spacing of 22.4 mm, covering the high frequency range from 1250 Hz to 6300 Hz. In order to ensure the perfectly phase match, the transfer function was determined after interchanging the microphone positions. The measurements were performed under relatively steady conditions of 39 ± 2% RH, 18 ± 2 °C and 1.01325×10^5 Pa. Three samples for each type of material were tested.

The main advantage of the impedance tube method relies on the possibility to test small samples. However, for practical use of coefficients, diffuse field values are usually needed, also accounting for different incidence angles. Such values are measured in a reverberant chamber and are known as Sabine absorption coefficients (α_{sab}) as defined by standard ISO 354 (2003). The method is based on an indirect estimation of the absorption coefficients depending on the measurements of the reverberation time T_{30} of the room before and after installing the test sample. The room was a 200 m^3 space with six non-parallel walls and a splayed ceiling. Additional diffusers having different shapes were added in order to increase diffusion. As the available maximum sample dimension was below the ISO standard requirements, ASTM C423-17 (2017) recommendations were taken as a reference and the test panels were placed on the room floor in two

different positions (Fig. 4). In particular, TW-68 and TW-96 materials were tested assembling an area of 5.76 m^2, in a shape of 2.40 by 2.40 m; whereas TW-134 material was tested assembling an area of 7.20 m^2, in a shape of 2.40 by 3.00 m. The measurement chain included an omni-directional sound source Look Line DL 301 and three microphones (two random incidence microphones GRAS 40-AR, one Neumann TLM 127 MT). Two source positions and twelve microphones positions per source were considered. The reverberation time of the full and empty room was calculated from impulse responses obtained by exciting the room with a 15 s logarithmic sine sweep from 50 to 7000 Hz. The difference between the two values of the measured reverberation time was used to calculate the equivalent sound absorption area of tested materials using the Sabine's formula. The α_{sab} coefficients were measured in one-third octave bands with center frequencies from 100 Hz to 5000 Hz. Air temperature and relative humidity, were continuously recorded in order to compute of air sound absorption according to ISO 9613-1 (1993).

2.2.4. Damping properties

The dynamic stiffness per unit of area *s'* of the tested nonwoven materials was experimentally determined using the resonant method according to ISO 9052-1 (1989). The method consisted in the measurement of the resonant frequency f_r of the fundamental vertical vibration of the mass-spring system formed by the load plate and the resilient material under test (Fig. 5(a)). The 20 × 20 cm test sample (three for each type of material) was placed between a steel inertial base plate and a steel load plate of 7.9 kg on which an accelerometer and a shaker were positioned. Only the mass of the top plate was considered as load system, because the mass of the accelerometer was negligible (i.e. 0.0125 kg) and an auxiliary suspension system of the shaker avoided its additional static load. The accelerometer DJB Instruments Type A/120/V fixed in the center of the top plate and connected to the computer via a charge amplifier made possible the vibration measurements. The shaker Signal force/Data Physics was used to excite the sample with a logarithmic sweep of 30 s, spanning from 5 to 300 Hz. The excitation force was controlled by an impedance head 288D01. The output signal from the accelerometer after excitation was analyzed with a custom MATLAB® script in order to detect the resonant frequency f_r of the sample under test. All measurements were analyzed with a frequency resolution of 0.2 Hz. The test allowed to determine the skeletal frame stiffness, also defined as the apparent dynamic stiffness of the material s_t'. As will be better explained later, the results of the air flow resistivity test were analyzed in order to evaluate whether the contribution of air stiffness s_a' had to be taken into account or not in dynamic stiffness measurement.

Once the dynamic stiffness was known, the *E*-modulus of the materials under test was computed as follows (Schiavi et al., 2005):

$$E = s' \bullet d \quad [1]$$

where *d* is the initial thickness of the material.

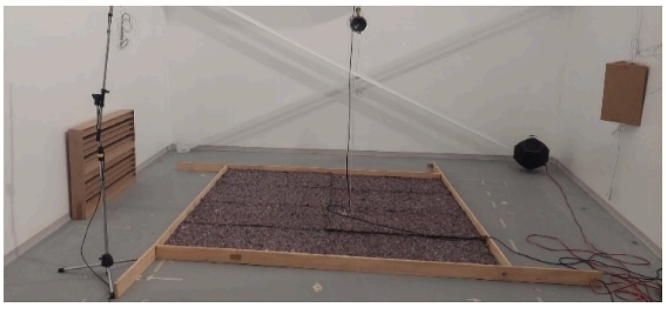

Fig. 4. Experimental investigation of the diffuse field sound absorbtion coefficients.

The measurement of the dynamic stiffness takes into account the mass-spring system resonant frequency only, neglecting the resonant width. Nonetheless, the bandwidth is related to the internal damping of a given building element, playing an important role in the reduction in impact sound pressure level. Thus, the Half-Power Point Method (Ewins, 1984) was followed to compute the loss factor η parameter from the width of the frequency response function at resonant peak. The frequencies f_1 and f_2 at −3 dB on the left and right of the resonant peak f_r were measured to determine η as follows:

$$\eta = \frac{f_2 - f_1}{f_r} \quad [2]$$

The compressibility, as well as the dynamic stiffness, is an important property to evaluate the ability of materials to reduce floor impact sound when used in floating floor structures. The extent of the crushing provoked by an instantaneous compression of the floating floor after a significant load is strictly dependent on the elasticity of a resilient underlayer. In fact, the resilient property of a material is influenced by its ability to recover the lost thickness after the overload action. The compressibility of the tested nonwovens was measured according to EN 12431 (2013) as the distance between a rigid flat base plate on which the test specimen was placed and a rigid flat pressure plate exerting different specified pressures on the top surface of the test specimen. In particular, thicknesses under different static load were measured: d_L, d_F and d_B were evaluated after applying static load respectively of 250 Pa, 2 kPa and 50 kPa, each for 120 s. The measurements were carried out by means of an INSTRON 5869 machine on three samples for each type of material. Compressibility *c* was expressed as the thickness obtained from the d_L-d_B difference. In order to evaluate the percentage thickness decrease, a non-dimensional quantity *h(c)* was also defined as follows:

$$h(c) = (1 - \xi) \bullet 100 \quad [3]$$

where ξ is the d_B on d_F ratio.

2.2.5. Thermal properties

The thermal insulation properties were experimentally investigated by means of the transient plane source device Isomet 2104 (Applied Precision Ltd). The tests were carried out at laboratory conditions of 21 ± 2 °C and 45 ± 5% RH, after oven drying the specimens to constant mass at 105 °C. Thermal conductivity λ, thermal diffusivity *D*, and volumetric heat capacity ρc_p were provided from the analysis of the temperature response of the material as a consequence of a heat flow impulse (Log and Gustafsson, 1995). The heat flow was induced by electrical heating of the resistor inserted in the surface probe in direct contact with the tested specimen (Fig. 5(b)). The specific heat capacity c_p was calculated from the measured volumetric heat capacity and bulk density.

2.3. Acoustic modelling

The non-acoustic properties were measured not only to characterize the microscopic structure and its effects on the sound absorption behaviour of the samples, but also to allow a better understanding of their acoustic response by the use of theoretical models. In this paper, the phenomenological model proposed by Johnson et al. (1987), taking into consideration the thermal integration suggested by Allard and Champoux (1992) and further modified by Lafarge et al. (1997) (later on referred as "JCAL" model) was considered to analyze and interpret the normal incidence sound absorption curves experimentally measured.

In 1987, Johnson et al. (1987) described the viscous-inertial dissipative effects in a saturated rigid frame porous medium introducing the effective density ρ_e which involved four characteristic parameters as the tortuosity τ, the open porosity ε, the air flow resistivity σ and the viscous characteristic length Λ:

Fig. 5. Experimental investigation of the dynamic stifness (a) and the thermal properties (b) of TW materials.

$$\rho_e = \frac{\tau\rho}{\varepsilon}\left[1 + \frac{\sigma\varepsilon}{j\omega\tau\rho}\sqrt{1 + j\frac{4\tau^2\eta\rho\omega}{\sigma^2\Lambda^2\varepsilon^2}}\right] \quad [4]$$

In 1992, Allard and Champoux (1992) completed the previous work developed by Johnson et al. (1987) introducing the dynamic bulk modulus K_e which took into account the thermal exchanges between a porous frame and its saturating fluid at high frequencies through the thermal characteristic length Λ'. Later, Lafarge et al. (1997) modified the dynamic bulk modulus K_e introducing the static thermal permeability k_0' in order to describe the low frequency behaviour of thermal effects:

$$K_e = \frac{\gamma P_0/\varepsilon}{\gamma - (\gamma - 1)\left[1 - j\frac{\varepsilon\eta}{k_0' N_P\rho\omega}\sqrt{1 + j\frac{4k_0'^2 N_P\rho\omega}{\eta\Lambda'^2\varepsilon^2}}\right]} \quad [5]$$

Direct measurement of the parameters used as input in the JCAL model is complex as a specific apparatus is required for each of them. To address this issue, the missing values were estimated by an inverse method (Atalla and Panneton, 2005) which took advantage of complex impedance measured in the tube. The values of the missing physical properties (i.e. tortuosity, viscous and thermal characteristic lengths and static thermal permeability) and of the directly measured ones (porosity and air flow resistivity), were determined by means of a search algorithm based on optimization techniques aimed to allow the best match between measurements and predictions. The algorithm was developed using the Matlab® software in order to explore properties which were not measurable over the entire range of possible values, while for measured parameters the range chosen considering their average values and taking into account their uncertainty. As the porosity was characterized by very low uncertainty, their measured values were directly used as input data of the JCAL model, allowing to speed up calculations. All the remaining input parameters, including air flow resistivity, which showed significant variations during measurements, were consequently estimated by the search algorithm.

Once the parameters were determined, it was possible to use theoretical formulas also to compute the effect of different incidence angles and, consequently, obtain the "diffuse field" values to compare with reverberation rom measurements. In order to increase the accuracy of the prediction, especially in the low frequency range, the finite size of the samples can be considered. In fact, assuming the surface of the materials as infinitely large, implies that the lateral dimensions of the sample are not very large compared to the wavelength. This assumption led to neglect any diffraction effects which occurred in normal practical applications, related to the outer free edges of the materials (Zhao et al., 2022). The *Alpha*Cell® software was used to compute the diffuse field values using the Finite Transfer Matrix Method (FTMM) proposed by Rhazi and Atalla (2010) allowing to consider the finite dimension of the sample. Thus, the infinite size radiation impedance in the receiving medium was replaced by the radiation impedance of a plane surface having the same shape and velocity distribution as the absorber tested in the reverberation room.

3. Results

3.1. Morphological properties

Fig. 6 shows results of SEM analysis, form which the porous network of randomly distributed fibers which characterized their microstructure clearly appeared. The morphological properties of TW-134 sample were reported considering that no relevant differences among the three materials were observed due to the small samples sizes needed for the SEM analysis. The fibrous matrix ensured a high void fraction in the studied nonwovens due to both the intra-fibers porosity corresponding to the voids inside the fibers and the inter-fibers porosity corresponding to the voids due to the fibers interlocking. Furthermore, the absence of any binding chemical agents avoided the full filling of the pores when binder solidified and the partial melting of bicomponent fibers only created bonding points.

Higher magnification SEM image (Fig. 6(b)) also allows to identify the smooth surface of Co PET/PET fibers used as binder from the other textile fibers. The textile wastes used as raw materials were selected among tailoring of the autumn-winter company collection; thus they resulted mainly of wool with a characteristic scaly surface pattern.

3.2. Non-acoustic properties

Table 2 outlines the results of the non-acoustic properties measured in the laboratory: the mean values of the open porosity ε and of the air flow resistivity σ are reported together with their measurement uncertainty expressed as the standard deviation of the mean (ISO/IEC Guide 98-3, 2008). The non-acoustic properties obtained from the inverse characterization are marked with a star.

The open structure previously observed in SEM images (Fig. 6) was proved by the measured open porosity values ranging from 0.92 for TW-68 with the lowest bulk density of 68 kg/m^3 to 0.89 for TW-134 with the highest bulk density of 134 kg/m^3. As it can be seen, the experimental results were robustly supported by the inverse characterization which provided ε* values with a maximum variation of about 2% with respect to ε ones.

With reference to the air flow resistivity, σ values ranged from 17.4 kN s/m^4 for the less dense TW-68 material to 95.5 kN s/m^4 for the denser TW-134 sample. During measurements, air flow resistivity values showed increased uncertainty than porosity and the σ* values provided by the inverse characterization differed from the measured σ values by a percentage ranging from approximately 9% for TW-68 sample to about 15% for TW-134.

The inverse algorithm allowed to characterize the geometric distribution of the pores, providing τ* values equal to unity for each tested sample. This meant a poor complexity of the path of the sound which

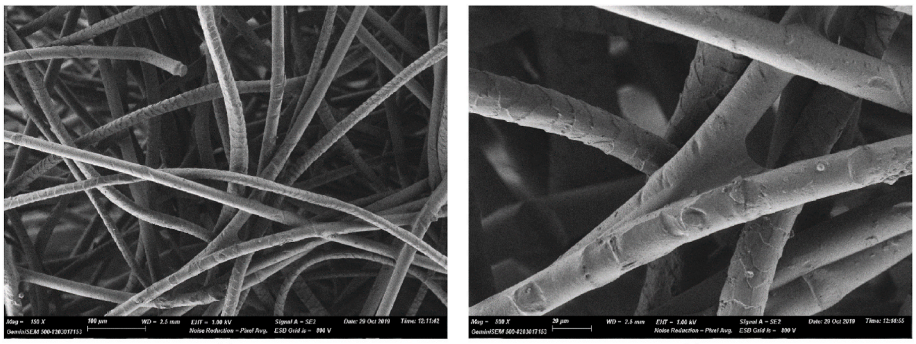

(a) (b)

Fig. 6. SEM images of TW-134 material at 150 X (a) and 500 X (b).

Table 2
Non-acoustic properties of TW samples resulting from the experimental measurements and determined with the inverse method. The last are marked with a star.

Parameters		TW-68	TW-96	TW-134
Porosity	ε [-]	0.92 ± 0.0019	0.91 ± 0.0016	0.89 ± 0.0016
Air flow resistivity	σ [kN·s/m^4]	17.4 ± 8.9	31.7 ± 8.6	95.5 ± 10.9
Porosity	ε^* [-]	0.92	0.89	0.87
Air flow resistivity	σ^* [kN·s/m^4]	19.2	38.0	81.2
Tortuosity	τ^* [-]	1.00	1.00	1.00
Viscous characteristic lengths	Λ^* [-]	5.07×10^{-5}	2.70×10^{-5}	1.67×10^{-5}
Thermal characteristic lengths	Λ'^* [-]	1.27×10^{-4}	5.94×10^{-5}	1.67×10^{-5}
Static thermal permeability	$k'_0{}^*$ [m^2]	2.1×10^{-9}	9.1×10^{-9}	9.1×10^{-9}

cross through the microstructure of the materials.

The viscous and thermal characteristic lengths and the static thermal permeability were also obtained applying the inverse method. As it can be observed, the predicted characteristic lengths ratio Λ'^*/Λ^* which could be considered as ratio of the characteristic dimension of pores interconnection to pores dimension, was 2.5 for TW-68, 2.2 for TW-96 and 1 for TW-134. The predicted value of the static thermal permeability was 2.1×10^{-9} for TW-68 and 9.1×10^{-9} for TW-96 and TW-134.

3.3. Sound absorption properties

Fig. 7 shows the normal incidence sound absorption curves measured in the impedance tube for each investigated material. The curves are plotted in one-third octave bands with center frequencies from 100 Hz to 6300 Hz.

A comparison among the experimental results pointed out that sample TW-68, more than any other that was tested, exhibited a sound absorption behaviour in accordance with the "ideal" performance of a porous material. In fact, the $\alpha\perp$ coefficients resulted to be very low in the low frequency range and sharply increased at medium and high frequencies, showing the first peak at 2125 Hz, with an $\alpha\perp$ value almost equal to unity. Such "ideal" acoustic behaviour observed for TW-68 could be expected due to its high porosity and low air flow resistivity values (i.e. $\varepsilon = 0.92$ and $\sigma^* = 19.2\text{kN·s/m}^4$) which favored a surface impedance more similar to that of the air. In addition, tortuosity close to the unity did not induce any shift in peak location which, in fact, occurred at a frequency exactly corresponding to a wavelength equal to four times the thickness of the sample.

Although TW-96 sample was characterized by a porosity $\varepsilon = 0.91$ and a predicted tortuosity value equal to the unity, it showed a sound

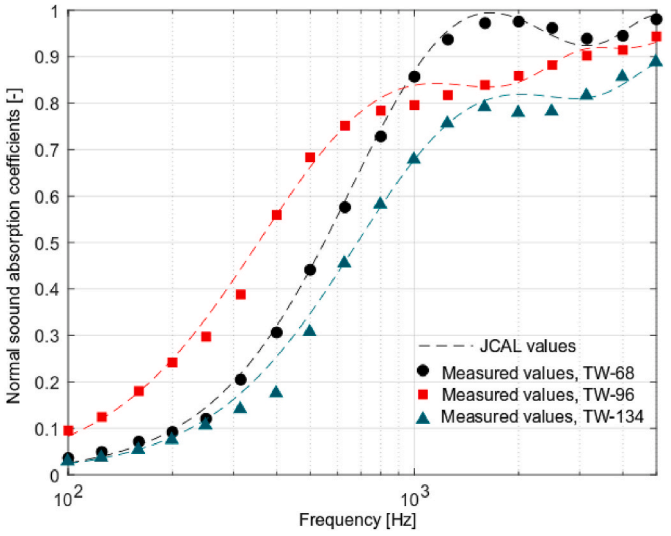

Fig. 7. Comparison between normal incidence sound absorption coefficients experimental measured and sound absorption curves predicted by JCAL model for TW-68, TW-96 and TW-134 samples with thicknesses respectively of 4 cm, 5 cm and 2.5 cm.

absorption curve without any evident peak. Likely, this could be explained by the high air flow resistivity value ($\sigma^* = 38.0\text{kN·s/m}^4$) which favored the sound energy loss by viscous and thermal friction, but, at the same time, the speed of sound through the samples decreased having effects on the reduction of the surface impedance of the material. In practice, the increased air flow resistivity led to an increase in absorption at low-medium frequencies at the cost of a decrease in absorption at high frequencies.

Similar considerations could apply to TW-134 which exhibited the highest air flow resistivity $\sigma^* = 81.2\text{kN·s/m}^4$. In this case, sound absorption coefficients were lower than TW-68 and TW-96 over the entire frequency range due to higher air flow resistivity value and decreased thickness of TW-134 sample.

The normal incidence sound absorption curves obtained from the experimental measurements were compared with those obtained using the JCAL model. As previously mentioned in Section 3.2, JCAL models were fed using the measured porosity values ε, while the values of the other parameters (i.e. air flow resistivity σ^*, tortuosity τ^*, shape factor s^*, characteristic lengths Λ^* and Λ'^* and static thermal permeability $k'_0{}^*$) were estimated by the inverse algorithm. Thus, the curve obviously represents the best possible approximation of experimental data that a model could provide. As it can be observed in Fig. 7, JCAL model predicted the normal incidence sound absorption for the TW-68 allowing a rather precise estimation of the first peak location, its height and width.

Thus, the mean absolute errors used to evaluate the accuracy of the JCAL model in predicting the sound absorption trend was 0.0127.

Some discrepancies between measured and predicted values could be appreciated for TW-96 and TW-134. In fact, for TW-96 JCAL model almost perfectly agreed with the experimental absorption coefficients in the medium-low frequency range up to 630 Hz, while in the high frequency range slight discrepancies appeared around 1 kHz. However, the mean absolute error remained very low, being 0.0170. Similarly, for TW-134 JCAL model showed almost perfected overlap with measured sound absorption coefficients up to 1600 Hz, but a few inaccuracies appeared in the high frequency range (with an absolute error of 0.0163). Such imperfect match observed for TW-96 and TW-134 may suggest that the model does not completely describe the nature of the real material.

Fig. 8, shows the absorption coefficients α_{sab} measured in the reverberation room plotted against the sound absorption curves calculated using *Alpha*Cell® with and without the finite size correction given by the application of the FTMM model (Rhazi and Atalla, 2010). The two curves were obtained using as input properties the values obtained by inversion of the JCAL dissipation model and assuming an infinitely motionless frame of the materials. As recommended by (Trevathan and Pearse, 2005), the actual diffuse field conditions can be better approximated by varying the angle of incidence from 0° to 82°. The absorption coefficients measured for each sample at normal incidence sound conditions were also given for reference.

As it was expected, α_{sab} coefficients were higher than $\alpha\perp$. Furthermore, α_{sab} measured for TW-68 and TW-96 in the medium-high frequency were higher than one. This is not unusual in a reverberant chamber and according to Scrosati et al. (2020), the main two reasons for this to happen may be the diffraction effects of the edges and the variation in the diffusivity of the sound field as a consequence of the sample placement. In fact, the presence of a highly absorbing sample could cause a change in the mean free paths of the sound waves in the room and a lack of reflections from the floor. In this way, the potential effects of shielding portions of room volume due to suspended diffuser panels may be emphasized. As suggested by literature (Shtrepi and Prato, 2020), the edge effect is more likely to happen for thicker panels.

However, independent of the measured values being higher than one, it is worth noticing that the sound absorption curves computed with *Alpha*Cell® software considering the finite size of the samples were in very good agreement with the curves measured in the reverberation room, and significantly better than those predicted assuming an infinite sample dimension. Similar results were expected because the infinite size of materials implied that the surface was so large in comparison to sound wavelength to neglect any edge effects which actually occurred on finite size samples.

3.4. Damping properties

The analysis of the resonant frequency f_r of the tested materials measured according to the normalized procedure, showed a dependence on the excitation force. In fact, f_r values linearly decreased when the amplitude of excitation force decreased. Therefore, the dynamic stiffness of all the samples was extrapolated at zero force, using a linear regression. Furthermore, as flow resistivity was within the range $10\ \mathrm{kN{\cdot}s/m^4} < \sigma < 100\ \mathrm{kN{\cdot}s/m^4}$ for all tested materials, the contribution due to air stiffness could not be neglected. In fact, during the dynamic stress of a porous sample characterized by open porosity and an "intermediate" air flow resistivity value, the air could remain trapped in the pores of the material making its elastic contribute not negligible (Schiavi et al., 2011). Therefore, in order to get correct measurement results consistent with standard requirements (ISO 9052-1, 1989), the total dynamic stiffness per unit area of the tested material s' was computed as a combination of the apparent dynamic stiffness per unit area s_t' and the stiffness of the air contained in open pores s_a' (Table 3). The average loss factor η calculated according to the Equation [2] was also given. As it

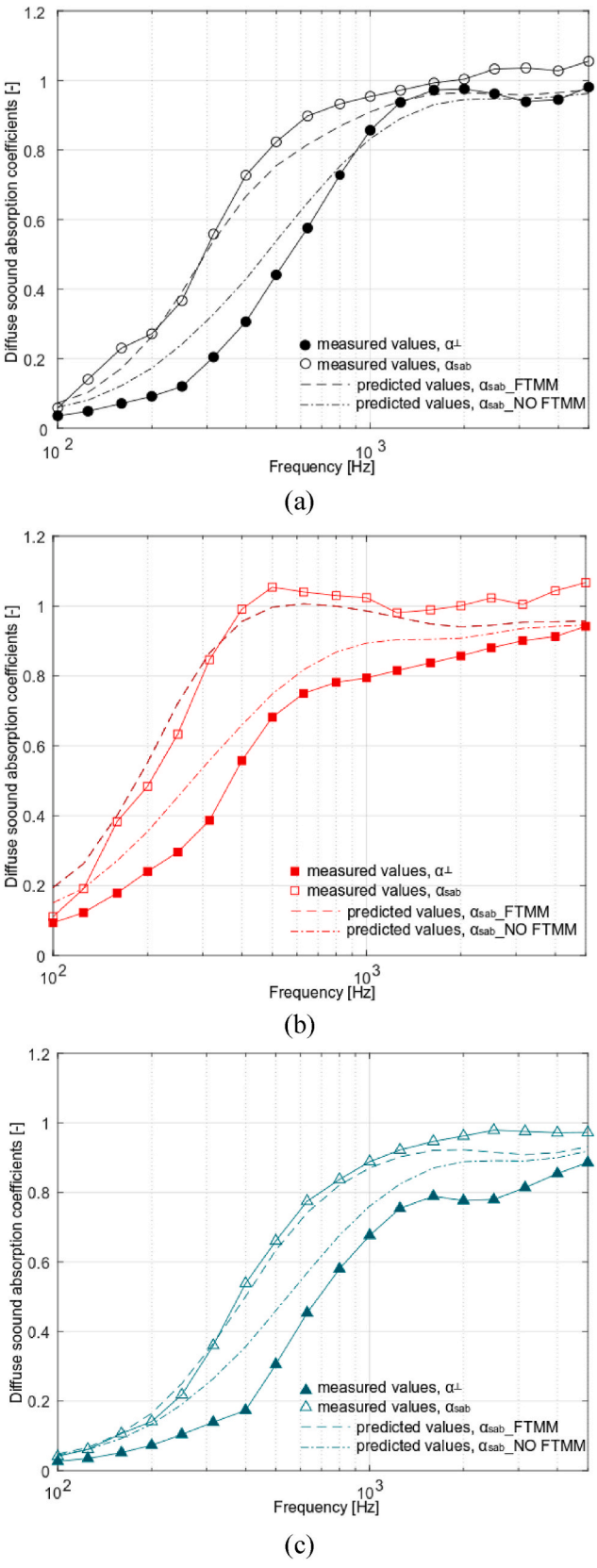

Fig. 8. Comparison between normal incidence sound absorption coefficients $\alpha\perp$ experimental measured and random incidence sound absorption coefficients α_{sab} measured in reverberation room and computed with *Alpha*Cell® 0.0 software considering or not the finite size correction (FTMM model) for TW-68 (a), TW-96 (b) and TW-134 (c) samples.

Table 3
Mean values of the measured total dynamic stiffness per unit area s' of the tested materials (with bulk density ρ_{bulk} and thickness d) extrapolated at zero force and computed as the sum of the apparent dynamic stiffness s_t' and the air dynamic stiffness s_a'. For each sample, the loss factor and the resonant frequency f_r expressed as mean value corresponding to zero force are reported.

Sample ID	TW-68	TW-96	TW-134
d [cm]	4.0	5.1	2.5
f_r [Hz]	27.3	25.3	33.1
s_t' [MN/m^3]	5.82	4.97	8.51
s_a' [MN/m^3]	2.75	2.23	4.55
s' [MN/m^3]	8.57	7.20	13.1
η [-]	0.22	0.24	0.27

can be observed, the average loss factor η of the tested materials ranged from 0.22 to 0.27, proving that they had a similar attitude to dissipate energy instead of radiating it as sound.

Table 4 shows the values of d_L, d_F and d_B measured in order to evaluate the compressibility c and the percentage thickness decrease $h(c)$ of the tested materials. As it can be seen, the compressibility of TW-68 and TW-96 samples was higher than that exhibited by TW-134. Thus, the TW-134 nonwoven resulted to be more suitable than the other two materials to be used as resilient underlayer in a floating floor structure. In fact, the $h(c)$ value of 11.5% showed that the material was able to recover most of the lost thickness after load cycles, more than TW-68 and TW-96 materials which showed an $h(c)$ value respectively of 20.5% and 14.6%. According to Caniato et al. (2016), materials with compressibility value up to about 5 mm could be considered good resilient layers.

3.5. Thermal properties

The parameters experimentally investigated to evaluate the thermal behaviour of the studied materials were the thermal conductivity λ, the thermal diffusivity D and the specific heat capacity c_p. The results of the experimental tests were summarized in Table 5, where these parameters are given with their uncertainty expressed as the standard deviation of the mean (ISO/IEC Guide 98-3, 2008).

Thermal conductivity proved to be strictly dependent on the bulk density values. In fact, the most lightweight materials showed a thermal conductivity of 0.040 W/(m·K) with a density of 68 kg/m^3, while λ value increased up to 0.050 W/(m·K) for the heaviest materials with 134 kg/m^3.

4. Discussion

4.1. Environmental advantages

One key point when discussing materials made of recycled components is whether their actual environmental impact is lower compared to conventional commercial materials. Obviously, this analysis would require a more detailed study which is under way and is beyond the scope of the present paper. Nonetheless, it is possible to make some general remarks that might help to understand the potential offered by a circular approach.

Table 4
Mean values of the thickness d_L, d_F and d_B measured under a static load respectively of 250 Pa, 2 kPa and 25 kPa for 120 s useful to calculate the compressibility and the percentage thickness decrease.

Sample ID	TW-68	TW-96	TW-134
d_L [mm]	33.49	44.45	20.48
d_F [mm]	24.15	34.73	17.59
d_B [mm]	19.20	29.67	15.57
c [mm]	33.49	14.78	4.91
$h(c)$ [%]	20.5	14.6	11.5

Table 5
Measured thermal properties of all tested materials: mean values of thermal conductivity λ, thermal diffusivity D, specific heat capacity c_p and their standard deviation of the mean (ISO/IEC Guide 98-3, 2008).

Sample ID	λ [W/(m·K)]	D [10^{-6} m^2/s]	c_p [J/(kg·K)]
TW-68	0.040 ± 0.0003	0.37 ± 0.016	1642 ± 88.8
TW-96	0.043 ± 0.0004	0.34 ± 0.013	1363 ± 63.5
TW-134	0.050 ± 0.0007	0.31 ± 0.013	1122 ± 42.5

The raw materials used to produce the panels are only two, i.e. the textile waste and the bi-component fibers, both coming from a waste collection and processing network. In fact, the textile fibers were pre-consumer waste discarded by the textile industry. Thus, being byproducts, the environmental impacts in terms of energy consumption during their production stage could be considered negligible. In addition, as they are subtracted to waste disposal processes, it has been demonstrated that an environmental advantage is certainly expected (Schmidt et al., 2016). The second raw material is copolyester/polyester fiber that, although being synthetic, can be produced from recycled plastic and circular processes, by means of low temperature depolymerization processes (Abbasi and Kotek, 2019; Guo et al., 2021).

Based on a preliminary LCA study, it was found that in terms of GHG emissions, the largest contributions come from polyester production from virgin fibers (accounting for about 60% of the overall emissions) and transportation of raw fibers (accounting for about 20% of the emissions). Anyway, in the first case, switching from hydrocarbon-based production to recycled polyester might reduce such impact to about 25%–50% of the emissions associated to conventional polyester production (Periyasamy and Militky, 2020). With reference to transport of the raw materials the distance between collection points and raw materials processing plays the major role (e.g. in Italy the number of processing establishments capable of treating textile waste is very limited and mostly located in Tuscany), and this might significantly affect the positive outcome of the analysis particularly when raw materials are collected in peripheral regions like Puglia. Thus, in a future perspective, building a proper industrial infrastructure that allows minimizing transportation costs, at least during the fabrication process, should be a primary objective for the success of such initiatives.

With reference to the energy demand during the fabrication (being responsible of 5% of GHG emissions), it is important to underline that, as shown in Fig. 2, most of the production line requires low energy to move machines, while the only part where heat is required is the heating and binding of the mixture that, thanks to bicomponent fibers, takes place at a low temperature (around 100 °C), which has a very low environmental impact as such process heat might result from renewable sources or from co-generation, thus with a near-to-zero impact in terms of carbon generation.

Lastly, regarding the end-of-life behaviour of the proposed samples, some concerns might arise about the disposal of the synthetic bi-component fibers. The presence of non-biodegradable synthetic materials hinders the decomposition of natural fibers, encouraging the landfill or the incineration of the textile waste (Pensupa, 2020). As consequence, the reuse of textile waste in form of mixed fibers for industrial products or filling could represent an added value in terms of environmental impact avoiding the use of not renewable materials (Schmidt et al., 2016). Clearly, in order to assure an effective recovery, it is necessary to recycle the fibers separately (Östlund et al., 2017). Yousef et al. (2020), tested an ecofriendly hydrophilicity solvent to distinguish polyester from cotton in jeans fabrics, demonstrating a significant CO_2 equivalent reduction of about 1448 kg per ton of waste compared to the usual approaches (i.e. landfilled and incineration).

4.2. Comparison with commercially available materials

Table 6 shows the measured properties of the tested panels together

Table 6
Comparison between thermal, acoustical and damping properties (i.e thermal conductivity λ, mean sound absorption coefficient $\alpha_{\perp m}$, air flow resistivity σ and dynamic stiffness s') of tested and commercially available materials (Hongisto et al., 2022).

Sample ID	ρ_{bulk} [kg/m^3]	λ [W/(m·K)]	σ [kN·s/m^4]	$\alpha_{\perp m}$ [-]	s' [MN/m^3]
TW-68	68	0.040	17.4	0.52	8.6
TW-96	96	0.043	31.7	0.56	7.2
TW-134	134	0.050	95.5	0.41	13.1
Stone wool	25 ÷ 100	0.033 ÷ 0.037	13 ÷ 50	0.56 ÷ 0.60	4.2 ÷ 16.0
Glass wool	16 ÷ 70	0.033 ÷ 0.035	12 ÷ 17	0.52 ÷ 0.58	3.0 ÷ 4.5
Wood fibers	50	0.038	8.8	0.50	6.6

with those of three commercially available thermal insulating materials (stone wool, glass wool and wood fibers) with comparable thickness of 5 cm. Thermal conductivity λ, mean sound absorption coefficient $\alpha_{\perp m}$, within 100 ÷ 3150 Hz, air flow resistivity σ and dynamic stiffness s' were considered for the comparison (Hongisto et al., 2022).

As it can be observed, TW panels showed conductivity values higher than conventional ones within a range from 5% to about 40% in the worst-case scenario (corresponding to the panel with highest density, which is less likely to be used for such applications). The mean sound absorption coefficients were also similar, being the air flow resistivity comparable (once again with the exception of TW-134), with the "sustainable" option being certainly easier to handle and to use, even without any further protective layer. Finally, also the values of the dynamic stiffness observed for TW panels were in agreement with those of commercially available materials, showing good damping performance. Therefore, it could be concluded that the TW panels could be used for real-world applications in place of the commercially available ones with just a small increase in thickness to obtain perfectly equivalent performance, but with a lower environmental impact.

4.3. Comparison between laboratory-scale and industrial-scale samples

TW samples were compared with the BICO samples previously characterized by the authors (Rubino et al., 2021) in order to assess opportunities and limitations of the upscaling process. The usual set of non-acoustic, acoustic and thermal properties were considered for comparison, proving that the industrial manufacturing process is capable of reproducing what was developed at laboratory scale (i.e. the mix proportion, the density value, etc.), producing materials with real world applications.

Considering the porosity of TW materials, the very porous matrix resulted in ε close to 0.9, which is in line with porosity values showed by BICO samples. In fact, despite the laboratory-scale process was likely to cause lower porosity ε values of BICO samples varied in the 0.96-0.86 range, while ρ_{bulk} values varied from 51 kg/m^3 to 167 kg/m^3.

The experimental results of the air flow resistivity observed for TW samples was also in accordance with the values measured for the BICO samples, but resistivity of the industrial-scale samples was lower than BICO for the lower density samples and higher for the highest density sample. In fact, BICO samples having ρ_{bulk} of 51, 90, or 136kg/m^3 showed measured air flow resistivity values respectively of 23.6, 44.9, or 69.4 kN s/m^4,differing, in the worst case, by up to 37% with respect to industrial-scale samples. Such differences are likely to be due to the industrial air-laying process which yields a less intricate microstructure unless the density is increased.

To support this finding, some interesting differences were observed with respect to the tortuosity values measured for BICO samples which resulted greater than the unity, especially for denser samples. In fact, BICO samples with ρ_{bulk} of 51kg/m^3 and 90kg/m^3 showed tortuosity values respectively of 1.32 and 1.09. When the density values of BICO materials increased, also their tortuosity increased showing values around 2 (i.e. 2.55, 1.82, and 2.16 respectively for samples with ρ_{bulk} of 167, 136 and 115 kg/m^3). On the contrary, TW materials exhibited tortuosity values equal to unity. Although the tortuosity values of the TW samples were predicted and those of the BICO materials were measured, it is reasonable to think that the dispersion of the batt waste in the airstream during the industrial-scale production process allowed to obtain a less intricate microstructure than that obtained following the laboratory-scale production technique.

As it can be observed in Fig. 9, the trend of the sound absorption coefficients observed for the TW-68 was similar to those measured for BICO-5 material with similar density and air flow resistivity values of 51kg/m^3 and 23.6kN·s/m^4, respectively. The sample BICO-5 showed better absorption capability at low-medium frequencies being 1 cm thicker than TW-68. The flatter curve shown by TW-96 was in accordance with the behaviour showed by BICO-4 sample with the same thickness, a density of 90kg/m^3 and air flow resistivity of 44.9kN·s/m^4. Direct comparisons between TW-134 and BICO samples were not possible due to difference in thickness.

Furthermore, the heat propagation ability observed for the investigated materials was in agreement with that observed for similar BICO nonwovens. In fact, BICO samples produced at laboratory scale showed a thermal conductivity values ranging from 0.044 to 0.057 W/(m·K). The higher specific heat capacity values observed for BICO samples ($1863 < c_p < 3544$ J/(kg·K)) compared to TW samples ($1122 < c_p < 1642$ J/(kg·K)) was again resulting from the different manufacturing process and affected the thermal diffusivity values, thus the ability to increase the temperature gradient in case of use of materials in practical applications. The D values showed by BICO samples ranged from 0.18×10^{-6} to 0.25×10^{-6} m^2/s, resulting slightly lower than those observed for the TW tested materials ($0.31 \times 10^{-6} < D < 0.37 \times 10^{-6}$ m^2/s). Therefore, a quicker rise of the temperature should be observed under unsteady conditions, when TW samples are used.

4.4. Practical implications

In order to further examine the practical applications of the studied panels also with reference to real world applications, and consequently in combination with other materials to be used in construction of new buildings or, more probably in the refurbishment of existing ones, the potential offered by *Alpha*Cell® software to model complex

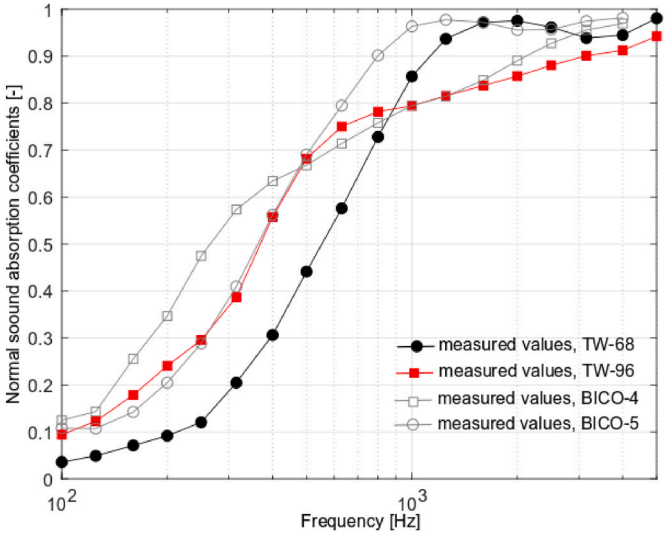

Fig. 9. Comparison between normal incidence sound absorption coefficients for TW-68 and BICO-5 samples, TW-96 and BICO-4 samples.

combinations of materials was exploited. In the light of the obtained experimental results, the thermal and acoustic performances of the tested materials TW-68 and TW-96 were investigated in relation to a reference masonry wall, whereas the potential of the TW-134 material was examined in relation to a reference concrete floor.

The transfer function method was used for determining the transmission coefficient τ in order to calculate the sound reduction index R (also known as sound transmission loss TL). The single-number sound transmission index R_w together with the adaptation terms C and C_{tr} was used in order to rate the airborne sound insulation capability with a single-number quantity instead of the whole frequency curve. The index R_w was determined by *Alpha*Cell® in accordance with the standardized methods (EN ISO 717-1, 2017).

The impact sound insulation potential especially of the TW-134 material was evaluated. In fact, any impact taking place on horizontal structures can stimulate vibrations which spread along the structure and are finally radiated as noise. The normalized impact sound pressure level L_n was computed by *Alpha*Cell® software with reference to all the damping properties, including the loss factor, previously obtained for each material (Section 3.4). As for airborne sound insulation, a single-number value L_{nw} may be used to rate the impact sound insulation properties, together with the adaptation term C_I which were obtained according to normalized methods (EN ISO 717-2, 2017).

The sound insulation offered by a building component, either for the airborne or impact sound depends by the radiation efficiency of the materials and by the actual excitation. Real partitions in buildings have finite size and receive sound energy from many angles at the same time. Therefore, in order to evaluate the sound insulating ability of the analyzed building components, a diffuse sound field with angles of incidences varying between 0° and 82° (i.e. between normal incidence and nearly grazing incidence) was considered and the results obtained taking into account the finite size of the absorbers were compared with those resulted for absorbers infinitely larger.

All materials were assumed as poro-elastic isotropic frames in which most of the sound energy was dissipated due to the vibration of pore walls and a minor part was temporarily stored. According to the Biot theory (Biot, 1992) the loss factor, Young's modulus E and Poisson's ratio υ are needed to describe the structural dissipation in isotropic materials.

In addition to acoustic properties, in order to better examine the thermal insulating performance of the tested materials and their effects on the insulating behaviour of the studied walls, the steady state thermal transmittance U and the surface mass M_S were calculated for each analyzed structure. Furthermore, the dynamic thermal properties as the periodic thermal transmittance Y_{mn} and its time shift Δt were computed according to EN ISO 13786 (2008) to evaluate thermal inertia of the considered structure, in order to evaluate its thermal performance, especially in cooling-dominated climates. The internal areal heat capacity κ was also determined to take into account the ability of building components to ensure indoor thermal comfort.

4.4.1. Modeling of acoustic and thermal insulation behaviour of a masonry structure

Fig. 10 shows the structures selected as examples to simulate the effects of adding the TW-68 and TW-96 layers in terms of enhancement of sound and thermal insulating behaviour of the walls. A wall consisting of clay bricks (6 × 12 × 25 cm) finished with mortar and gypsum plaster 1.5 cm thick on both sides was chosen as reference structure named "base". In the configuration named "coat" the TW layer was added on the internal side of the reference wall; in the configuration named "gap" the TW material was interposed between two layers of clay bricks respectively 6 cm and 12 cm thick. The TW materials were used considering their real thickness in order to characterize them by referring to the experimental measurements results. Thus TW-68 material was 4 cm thick; whereas TW-96 material was 5 cm thick.

In Table 7 the layers and their thermal and elastic properties used in the selected walls are summarized. Both thermal and elastic properties of the gypsum plaster, the clay bricks and the plasterboard were taken from technical datasheets or from software material libraries. Conversely, the properties of the TW materials were specifically determined. Particularly, the loss factor η values were directly determined from the dynamic stiffness measurements as discussed above in Section 3.4; whereas Young's modulus E was determined following the Equation [1]. Furthermore, being the TW samples constituted by most of fibers assumed to be parallel to the material plane, Poisson's ratio υ determined for normal compression was assumed to be zero and frequency independent (Dauchez et al., 2002). The thermal conductivity and the specific heat capacity were directly measured as previously discussed in Section 3.5.

Fig. 11 shows the improvements of transmission loss changes with frequency when TW materials were added to reference wall structure. The ΔTL value was calculated as the difference between the transmission loss TL of the "gap" and "coat" structures with TW-68 and TW-96 layers and those of the "base" wall. The addition of TW materials in both

Table 7
Input materials properties to simulate the thermic and acoustic insulating behaviour of a masonry structure: bulk density ρ_{bulk}, loss factor η, modulus of elasticity E, Poisson's ratio υ, thermal conductivity λ and specific het capacity c.

Item	Material	ρ_{bulk} [kg/m^3]	η [-]	E [N/m^2]	υ [-]	λ [W/(m·K)]	c [J/(kg·K)]
1	Gypsum plaster	1700	0.01	2.5×10^9	0.20	0.700	1000
2	Clay brick	1500	0.01	1.4×10^{10}	0.20	0.720	1000
3	TW-68	68	0.22	2.3×10^5	0	0.040	1642
3	TW-96	96	0.24	2.5×10^5	0	0.043	1363
4	Plasterboard	800	0.05	3.2×10^9	0.30	0.210	1000

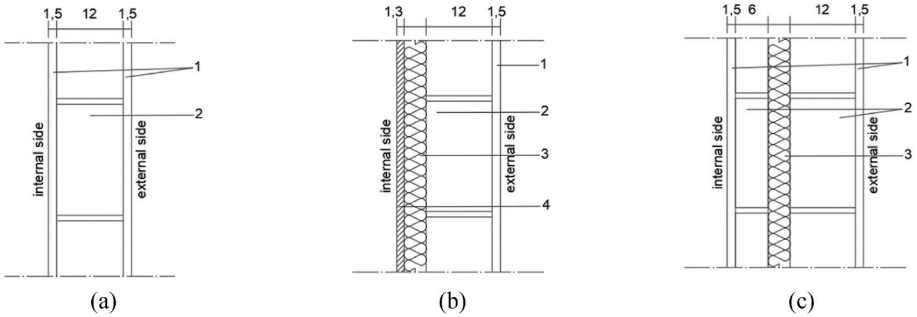

Fig. 10. Configurations of masonry structure simulated to compare the sound insulation of a reference wall (a) with walls that involved the addition of layers of TW material on one side (b) or inside (c). TW-68 and TW-96 materials were 4 cm and 5 cm thick, respectively.

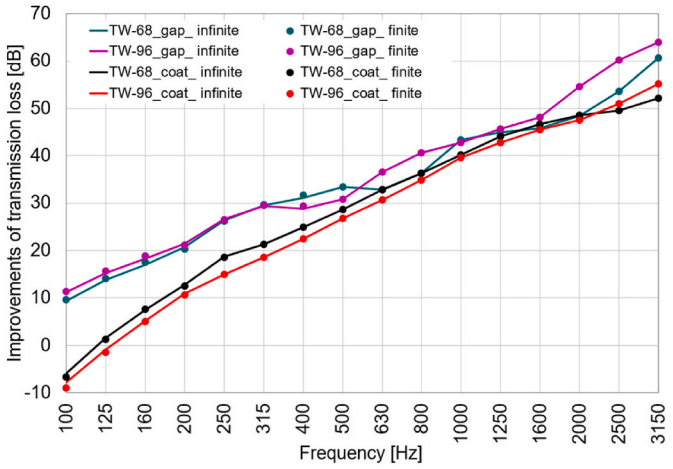

Fig. 11. Comparison of improvements of transmission loss changes for coat configuration and gap one.

configurations ("coat" or "gap") led to *TL* improvements over the entire frequency range. This was positively expected as the fibrous layer behaves as a spring in mass-spring-mass system that start improving *R* from the resonance frequency on and, given the large amount of air that the fibrous layer incorporates, the resonance frequency could be predicted to be low. This meant greater sound insulating properties of the walls with the extra TW layer which better prevented the sound waves from being transmitted.

Furthermore, the curves obtained assuming an infinitely large sample were compared with those considering a finite size of the wall (corresponding to 3 m × 4 m). As it can be observed, no evident differences could be found.

Table 8 summarized the single-number sound transmission index R_w together with the adaptation terms C and C_{tr} used to evaluate the airborne sound insulation of the analyzed masonry structures. ΔR_w returns the increase in sound insulating performance due to the addition of TW layers. As expected, R_w obtained for the "gap" configurations resulted higher than those for the "coat" ones. In fact, the mass-spring-mass system obtained interposing the elastic TW cavity between two massive brick layers was more efficient to attenuate the transmission of the acoustic energy.

In order to evaluate the effects of the addition of the insulating layer on the thermal behaviour of the analyzed structures, the stationary thermal transmittance U, the periodic thermal transmittance Y_{mn}, the time shift Δt and the internal areal heat capacity κ evaluated according to EN ISO 13786 (2008) were given in Table 9.

As it can be seen, the tested TW materials behaved as good thermal insulators, leading to an important reduction of the stationary and the periodic thermal transmittance. This last Y_{mn} parameter assumed very low values for "gap" configuration, highlighting the possibility of using TW nonwovens as cavity filling materials able to ensure a reduction in the impact of outside thermal load, particularly from direct sunlight irradiation on the external walls. Furthermore, it could be possible to guarantee a good κ value (higher than the minimum value of 40 [kJ/(m^2 K)] imposed by the Italian regulations Decree, October 11, 2017) useful to reduce the contribution of the internal loads, developing envelopes very efficient in relation to indoor comfort.

Table 9
Surface mass M_S, stationary thermal transmittance U, periodic thermal transmittance Y_{mn}, time shift Δt and internal areal heat capacity κ evaluated according to EN ISO 13786 (2008) for base, coat and gap configurations obtained adding TW-68 and TW-96 materials.

Configuration	M_S [kg/m^2]	U [W/(m^2 K)]	Y_{mn} [W/(m^2 K)]	Δt [h]	κ [kJ/(m^2 K)]
base	231	2.630	0.764	8.31	77.456
coat_TW-68	219	0.704	0.123	9.11	12.945
gap_TW-68	324	0.684	0.019	15.49	98.629
coat_TW-96	221	0.632	0.108	9.13	11.530
gap_TW-96	326	0.615	0.017	15.52	98.641

4.4.2. Modeling of acoustic insulating behaviour of a concrete floor

Fig. 12 shows the floor structures selected to simulate with the *Alpha*Cell® software the effects of adding TW-134 layer in terms of reducing the impact sound transmission. A solid concrete floor consisting of a 14 cm thick dense concrete slab and a walking surface of 5 cm thick concrete screed and PVC floor tiles was chosen for the reference structure named "base". The "floating" configuration involved the addition of the elastic TW material between the dense concrete slab and the walking surface.

In Table 10 the layers and their elastic properties used in the selected floors are outlined. As for modeling the insulating behaviour of masonry structures, only the properties of the TW-134 material were specifically determined; whereas the properties of the rest of used materials were taken from product technical datasheets or from software material library.

Fig. 13 shows the effect of the addition of the resilient layer on the impact sound pressure transmission through the concrete slab. In particular, the impact sound insulation improvement is plotted in terms of ΔL_n value calculated as the difference between the normalized impact sound pressure level L_n of the "base" floor and those of the "floating" structure. The mass-spring-mass system formed by the slab-resilient layer-walking surface system allowed to obtain a decreasing in the L_n value over the entire frequency range, reducing the generated impact sound pressure level. As previously explained, negligible differences could be observed between the curves obtained assuming an infinitely large sample and those considering a finite size of the floor (corresponding to 3 m × 4 m).

The single-number impact sound pressure level $L_{n,w}$ reported together with the adaptation term C_I in Table 11 confirmed the positive role played by the TW material. In fact, the TW material acted as a resilient underlayer able to damp the impact sound generated by footsteps, object fall and so on. Table 11 also shows the $L_{n,w}$ obtained as the difference between the single-number impact sound pressure level of the "base" slab and those of the "floating" structure with the resilient material installed.

Table 8
Single-number sound transmission index R_w together with the adaptation terms C and C_{tr} and ΔR_w values. The values reported are referred to the case of finite and infinite surface of the masonry structure.

Configuration	R_w [dB]		C [dB]		C_{tr} [dB]		ΔR_w [dB]	
	Finite	Infinite	Finite	Infinite	Finite	Infinite	Finite	Infinite
base	43	42	−1.0	−2.0	−4.0	−5.0	–	–
coat_TW-68	61	58	−3.0	−4.0	−10.0	−10.0	18	16
gap_TW-68	71	68	−4.0	−4.0	−9.0	−10.0	25	23
coat_TW-96	60	58	−3.0	−3.0	−9.0	−10.0	17	16
gap_TW-96	71	68	−3.0	−4.0	−8.0	−9.0	25	23

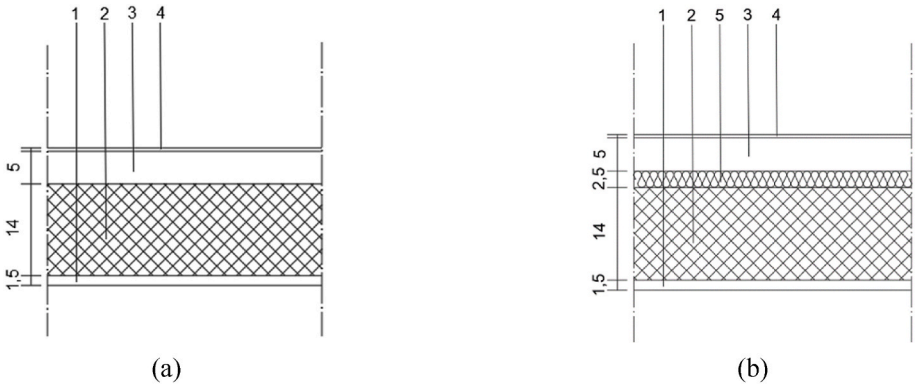

Fig. 12. Floor configurations simulated in *Alpha*Cell® software to compare the sound insulation of a reference concrete floor (a) with a floating floor involving the addition of a TW layer (b).

Table 10
Input materials properties to simulate the thermal and acoustic insulating behaviour of a masonry structure: bulk density ρ_{bulk}, loss factor η, modulus of elasticity E, Poisson's ratio υ.

Item	Material	ρ_{bulk} [kg/m^3]	η [-]	E [N/m^2]	υ [-]
1	Gypsum plaster	1700	0.01	2.5×10^9	0.20
2	Concrete slab	2321	Frequency dependent	3.5×10^{10}	0.23
3	TW-134	134	0.27	2.1×10^5	0
4	Concrete screed	1400	0.01	2.5×10^9	0.20
5	PVC tiles	1000	0.20	2.1×10^8	0.3

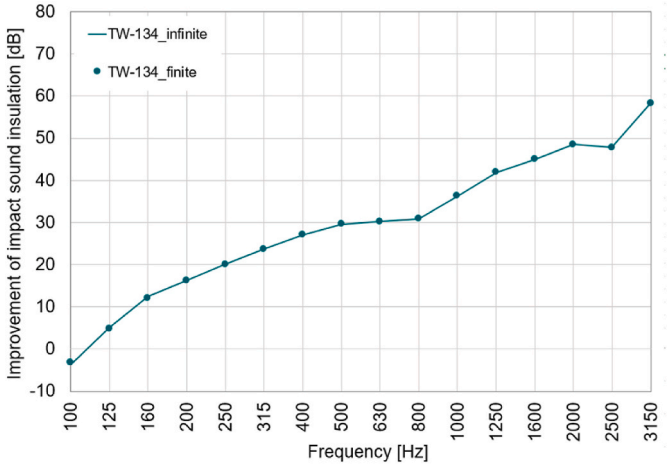

Fig. 13. Improvement of impact sound insulation when TW-134 material was added to the "base" floor.

Table 11
Normalized single-number sound pressure level $L_{n,w}$ together with the adaptation term C_I and $\Delta L_{n,w}$ values. The values reported are referred to the case of finite and infinite surface of the masonry structure.

Configuration	$L_{n,w}$ [dB]		C_I [dB]		$\Delta L_{n,w}$ [dB]	
	Finite	Infinite	Finite	Infinite	Finite	Infinite
base	62	64	−0.5	0.9	–	–
floating_TW-134	50	55	−3.0	−3.0	12	9

5. Conclusions

The present paper investigates the thermal and acoustic properties of an industrial scale-up of building materials made of textile wastes with the aim of complementing a preliminary research (Rubino et al., 2021) in which similar building nonwovens (referred to as "BICO") were produced at a laboratory scale using same raw materials. Several panels differing in density and thickness values were developed, following an industrial airstream production process and their thermal, acoustic and damping properties were characterized. The experimental results were compared with those collected in (Rubino et al., 2021) in order to verify that the industrial manufactured process allowed to obtain products that could find practical application, while preserving the promising thermal insulation and sound absorption performance previously observed. The main findings were.

- the scanning electron microscopy investigation of the porous microstructure of the materials highlighted their open cell structure thanks to their fibrous nature. The open cell structure justified porosity values close to 0.9 as observed for the previously produced BICO samples;
- all the samples showed an air flow resistivity lower than 100 kN s/m^4 and a tortuosity close to the unity. The industrial-scale production process influenced the fibers matrix, making it less intricate than that obtained following the laboratory-scale production technique;
- good sound absorption coefficients at normal and random incidence were measured for all the materials. The obtained curves were in agreement with the theoretical trends and with the behaviours exhibited by BICO materials with similar density and air flow resistivity values;
- all the nonwovens showed damping properties (i.e. dynamic stiffness and compressibility) to be used for improving sound insulation of buildings;
- the analysis of the thermal properties revealed that the tested materials could easily compete with traditional insulators, showing a thermal conductivity less than 0.05 W/(m·K). Similar results were obtained for the BICO materials.

In light of the above mentioned results and of the acoustic and thermal insulating behaviour observed after applying the materials to examples of walls, the proposed materials might be conveniently proposed to fill air gaps in masonry walls, or as internal finishing. Furthermore, the damping properties similar to those of conventional materials and the good behaviour observed for a concrete floor including the studied nonwovens, suggested the possibility of using especially one of them as valid resilient layers in a floating floor.

CRediT authorship contribution statement

Chiara Rubino: Conceptualization, Methodology, Validation, Formal analysis, Investigation, Data curation, Writing – original draft, Writing – review & editing, Visualization. **Stefania Liuzzi:** Conceptualization, Methodology, Validation, Formal analysis, Investigation, Data curation, Writing – review & editing. **Pietro Stefanizzi:** Conceptualization, Methodology, Validation, Formal analysis, Investigation, Resources, Writing – review & editing, Supervision. **Francesco Martellotta:** Conceptualization, Methodology, Software, Validation, Formal analysis, Investigation, Resources, Writing – review & editing, Supervision, Project administration, Funding acquisition.

Declaration of competing interest

The authors declare that they have no known competing financial interests or personal relationships that could have appeared to influence the work reported in this paper.

Data availability

Data will be made available on request.

Acknowledgments

Authors thank the financial support of the Italian PRIN ("Progettodi Ricerca di Rilevante Interesse Nazionale) Project "SUSTAIN/ABLE e SimultaneoUs STructural And energetIc reNovAtion of BuiLdings through innovativE solutions", ERC Sector PE8, ID20174RTL7W. Authors acknowledge the "Hackustica" start-up for the support during the manufacturing process of the panels. Furthermore, authors thank Francesco Paparella for his contribution during the compressibility tests.

References

Abbasi, M., Kotek, R., 2019. Effects of drawing process on crimp formation-ability of side-by-side bicomponent filament yarns produced from recycled, fiber-grade and bottle-grade. PET. J. Text. Inst. 110 (10), 1439–1444. https://doi.org/10.1080/00405000.2019.1611523.

Allard, J.F., Champoux, Y., 1992. New empirical equation for sound propagation in rigid frame fibrous material. J. Acoust. Soc. Am. 91, 3346–3353. https://doi.org/10.1121/1.402824.

Antolinc, D., Eleršic Filipic, K., 2021. Recycling of nonwoven polyethylene terephthalate textile into thermal and acoustic insulation for more sustainable buildings. Polymers 13, 3090. https://doi.org/10.3390/polym13183090.

ASTM C423-17, 2017. Standard Test Method for Sound Absorption and Sound Absorption Coefficients by the Reverberation Room Method. ASTM International, West Conshohocken, USA.

Atalla, Y., Panneton, R., 2005. Inverse acoustical characterization of open cell porous media using impedance tube measurements. Can. Acoust. 33 (1), 11–24 jcaa.caa-aca.ca/index.php/jcaa/article/view/1711.

Atiénzar-Navarro, R., Bonet-Aracil, M., Gisbert-Payá, J., del Rey, R., Picó, R., 2022. Influence of fineness, length and hollow section of fibers on acoustic absorption. Textil. Res. J. 92 (3–4), 400–408. https://doi.org/10.1177/00405175211036200.

Belakroum, R., Gherfi, A., Bouchema, K., Gharbi, A., Kerboua, Y., Kadja, M., Maalouf, C., Mai, T.H., El Wakil, N., Lachi, M., 2017. Hygric buffer and acoustic absorption of new building insulation materials based on date palm fibers. J. Build. Eng. 12, 132–139. https://doi.org/10.1016/j.jobe.2017.05.011.

Berardi, U., Iannace, G., 2015. Acoustic characterization of natural fibers for sound absorption applications, Build. Environ. Times 94, 840–852. https://doi.org/10.1016/j.buildenv.2015.05.029.

Binici, H., Eken, M., Dolaz, M., Aksogan, O., Kara, M., 2014. An environmentally friendly thermal insulation material from sunflower. Construct. Build. Mater. 51, 24–33. https://doi.org/10.1016/j.conbuildmat.2013.10.038.

Biot, M.A., 1992. In: Biot, M.A. (Ed.), Acoustic, Elasticity, and Thermodynamics of Porous Media-Twenty-One Papers. I. Tolstoy ~American Institute of Physics, Woodbury, NY.

Briga-Sá, A., Nascimento, D., Teixeira, N., Pinto, J., Caldeira, F., Varum, H., Paiva, A., 2013. Textile waste as an alternative thermal insulation building material solution. Construct. Build. Mater. 38, 155–160. https://doi.org/10.1016/j.conbuildmat.2012.08.037.

Caniato, M., Bettarello, F., Marsich, L., Ferluga, A., Sbaizero, O., Schmid, C., 2016. Time-depending performance of resilient layers under floating floors. Construct. Build. Mater. 102, 226–232. https://doi.org/10.1016/j.conbuildmat.2015.10.176.

Czajkowski, Ł., Kocewicz, R., Weres, J., Olek, W., 2022. Estimation of thermal properties of straw-based insulating panels. Mater 15 (3), 1073. https://doi.org/10.3390/ma15031073.

Dauchez, N., Etchessahar, M., Sahraoui, S., 2002. On Measurement of Mechanical Properties of Sound Absorbing Materials. 2nd Biot Conference on Poromechanics, Grenoble, France, pp. 1–4.

Decree, Ministerial, 11 October, 2017. Criteri ambientali minimi per l'affidamento di servizi di progettazione e lavori per la nuova costruzione, ristrutturazione e manutenzione di edifici pubblici. GU Serie Generale n, 259 del 06-11-2017.

Directive 2002/91/EC, 2002. European Parliament and of the Council of 16 December 2002 on the energy performance of buildings. Official Journal of European. Communities 2003: L 1/65. https://eur-lex.europa.eu/legal-content/EN/TXT/PDF/?uri=CELEX:32002L0091&from=EN.

Directorate-General for Communication (European Commission), 2020. Circular Economy Action Plan: for a Cleaner and More Competitive Europe. Publications Office of the European Union, Luxembourg, ISBN 978-92-76-19070-7.

EN 12431, 2013. Thermal Insulating Products for Building Applications-Determination of Thickness for Floating Floor Insulating Products. International Organization for Standardization, Geneva, Switzerland.

EN ISO 13786, 2008. Thermal performance of building components. In: Dynamic Thermal Characteristics. Calculation methods; International Organization for Standardization, Geneva, Switzerland.

EN ISO 717-1, 2017. Acoustics - Rating of Sound Insulation in Buildings and of Building Elements - Part 1: Air Borne Sound Insulation. International Organization for Standardization, Geneva, Switzerland.

EN ISO 717-2, 2017. Acoustics - Rating of Sound Insulation in Buildings and of Building Elements - Part 1: Impact Sound Insulation. International Organization for Standardization, Geneva, Switzerland.

Ewins, D.J., 1984. Modal Testing: Theory and Practice. Research studies press, Letchworth.

Ghermezgoli, Z.M., Moezzi, M., Yekrang, J., Rafat, S.A., Soltani, P., Barez, F., 2021. Sound absorption and thermal insulation characteristics of fabrics made of pure and crossbred sheep waste wool. J. Build. Eng. 35, 102060 https://doi.org/10.1016/j.jobe.2020.102060.

Guo, Z., Warlin, N., Mankar, S.V., Sidqi, M., Andersson, M., Zhang, B., Nilsson, E., 2021. Development of circularly recyclable low melting temperature bicomponent fibers toward a sustainable nonwoven application. ACS Sustainable Chem. Eng. 2021 9 (49), 16778–16785. https://doi.org/10.1021/acssuschemeng.1c06302.

Hongisto, V., Saarinen, P., Alakoivu, R., Hakala, J., 2022. Acoustic properties of commercially available thermal insulators - an experimental study. J. Build. Eng. 54, 104588 https://doi.org/10.1016/j.jobe.2022.104588.

Ingard, U.K., Dear, T.A., 1985. Measurement of acoustic flow resistance. J. Sound Vib. 103 (4), 567–572. https://doi.org/10.1016/S0022-460X(85)80024-9.

ISO 10534-2, 1998. Acoustics - Determination of Sound Absorption Coefficient and Impedance in Impedance Tubes - Part 2: Transfer-Function Method. International Organization for Standardization, Geneva, Switzerland.

ISO 354, 2003. Acoustics - Measurement of Sound Absorption in a Reverberation Room. International Organization for Standardization, Geneva, Switzerland.

ISO 9052-1, 1989. Acoustics - Determination of Dynamic Stiffness - Part 1: Materials Used under Floating Floors in Dwellings. International Organization for Standardization, Geneva, Switzerland.

ISO 9613, 1993. Acoustics – Attenuation of Sound during Propagation Outdoors – Part 1: Calculation of the Absorption of Sound by the Atmosphere. International Organization for Standardization, Geneva, Switzerland.

ISO/IEC Guide 98-3, 2008. Uncertainty of measurement e Part 3: Guide to the expression of uncertainty in measurement (GUM:1995). International Organization for Standardization, Geneva, Switzerland.

Ji, X., Zhang, H., Bai, Z., Qiu, G., Guo, M., Cheng, F., Zhang, M., 2019. Self-assembled multifunctional bulk hollow microspheres: thermal insulation, sound absorption and fire resistance. Energy Build. 205, 109533 https://doi.org/10.1016/j.enbuild.2019.109533.

Johnson, D.L., Koplik, J., Dashen, R., 1987. Theory of dynamic permeability and tortuosity in fluid-saturated porous media. J. Fluid Mech. 176, 379–402. https://doi.org/10.1017/S0022112087000727.

Kamble, Z., Behera, B.K., 2021. Sustainable hybrid composites reinforced with textile waste for construction and building applications. Construct. Build. Mater. 284, 122800 https://doi.org/10.1016/j.conbuildmat.2021.122800.

Karimi, F., Soltani, P., Zarrebini, M., Hassanpour, A., 2022. Acoustic and thermal performance of polypropylene nonwoven fabrics for insulation in buildings. J. Build. Eng. 50, 104125 https://doi.org/10.1016/j.jobe.2022.104125.

Kaushik, A., Arif, M., Prasad, T., John Ebohon, O., 2020. Effect of thermal comfort on occupant productivity in office buildings: response surface analysis. Build. Environ. 180, 107021 https://doi.org/10.1016/j.buildenv.2020.107021.

Khan, N.A., Bhattacharjee, B., 2021. Thermal and noise insulation performance interaction of building envelope during building simulation optimization in tropical climates. Build. Environ. 200, 107948 https://doi.org/10.1016/j.buildenv.2021.107948.

Lacoste, C., El Hage, R., Bergeret, A., Corn, S., Lacroix, P., 2018. Sodium alginate adhesives as binders in wood fibers/textile waste fibers biocomposites for building insulation. Carbohydr. Polym. 184, 1–8. https://doi.org/10.1016/j.carbpol.2017.12.019.

Lafarge, D., Lemarinier, P., Allard, J.-F., Tarnow, V., 1997. Dynamic compressibility of air in porous structures at audible frequencies. J. Acoust. Soc. Am. 102 (4), 1995–2006. https://doi.org/10.1121/1.419690.

Liao, J., Zhang, S., Tang, X., 2020. Sound absorption of hemp fibers (cannabis sativa l.) based nonwoven fabrics and composites: a Review. J. Nat. Fibers 19 (4), 1297–1309. https://doi.org/10.1080/15440478.2020.1764453.

Liuzzi, S., Rubino, C., Stefanizzi, P., Martellotta, F., 2020. Performance characterization of broad band sustainable sound absorbers made of almond skins. Mater 13 (23), 5474. https://doi.org/10.3390/ma13235474.

Log, T., Gustafsson, S.E., 1995. Transient plane source (TPS) technique for measuring thermal transport properties of building materials. Fire Mater. 19, 43–49. https://doi.org/10.1002/fam.810190107.

Lu, W., Chi, B., Bao, Z., Zetkulic, A., 2019. Evaluating the effects of green building on construction waste management: a comparative study of three green building rating systems. Build. Environ. 155, 247–256. https://doi.org/10.1016/j.buildenv.2019.03.050.

Martellotta, F., Cannavale, A., De Matteis, V., Ayr, U., 2018. Sustainable sound absorbers obtained from olive pruning wastes and chitosan binder. Appl. Acoust. 141, 71–78. https://doi.org/10.1016/j.apacoust.2018.06.022.

Mehrzad, S., Taban, E., Soltani, P., Samaei, S.E., Khavanin, A., 2022. Sugarcane bagasse waste fibers as novel thermal insulation and sound-absorbing materials for application in sustainable buildings. Build. Environ. 211, 108753 https://doi.org/10.1016/j.buildenv.2022.108753.

Östlund, A., Syren, P.O., J€onsson, C., Ribitsch, D., Syren, M., 2017. Re:MixeSeparation and Recycling of Textile Waste Fiber Blends. MISTRA Future Fashion report, Rise: Borås, Sweden.

Pensupa, N., 2020. Recycling of end-of-life clothes. In: Rajkishore, N. (Ed.), Sustainable Technologies for Fashion and Textiles. Woodhead Publishing Series in Textiles, United Kingdom, p. 251e309.

Periyasamy, A.P., Militky, J., 2020. LCA (life cycle assessment) on recycled polyester. In: Muthu, S. (Ed.), Environmental Footprints of Recycled Polyester. Textile Science and Clothing Technology. Springer, Singapore. https://doi.org/10.1007/978-981-13-9578-9_1.

Rhazi, D., Atalla, N., 2010. A simple method to account for size effects in the transfer matrix method. JASA Express Letters 127 (2), EL30–EL36. https://doi.org/10.1121/1.3280237.

Rubino, C., Bonet Aracil, M., Liuzzi, S., Stefanizzi, P., Martellotta, F., 2021. Wool waste used as sustainable nonwoven for building applications. J. Clean. Prod. 278, 123905 https://doi.org/10.1016/j.jclepro.2020.123905.

Sakthivel, S., Kumar, S.S., Melese, B., Mekonnen, S., Solomon, E., Edae, A., Abedom, F., Gedilu, M., 2021. Development of nonwoven composites from recycled cotton/polyester apparel waste materials for sound absorbing and insulating properties. Appl. Acoust. 180, 108126 https://doi.org/10.1016/j.apacoust.2021.108126.

Samanta, K.K., Mustafa, I., Debnath, S., Das, E., Basu, G., Ghosh, S., 2021. Study of thermal insulation performance of layered jute nonwoven: a sustainable material. J. Nat. Fibers 1–14. https://doi.org/10.1080/15440478.2020.1856274.

Schiavi, A., Pavoni Belli, A., Russo, F., 2005. Estimation of acoustical performance of floating floors from dynamic stiffness of resilient layers. Bouild. Acoust. 12 (2) https://doi.org/10.1260/1351010054037938, 2005.

Schiavi, A., Guglielmone, C., Miglietta, P., 2011. Effect and importance of static-load on airflow resistivity determination and its consequences on dynamic stiffness. Appl. Acoust. 72, 705–710. https://doi.org/10.1016/j.apacoust.2011.03.009.

Schmidt, A., Watson, D., Roos, S., Askham, C., Brunn Poulsen, P., 2016. Mixed Fibres in: Gaining Benefits from Discarded Textiles. Rosendahls-Schultz Grafisk, Hillerød, Denmark, p. 112e116.

Scrosati, C., Martellotta, F., Pompoli, F., Schiavi, A., Prato, A., D'Orazio, D., Garai, M., Granzotto, N., Di Bella, A., Scamoni, F., Depalma, M., Marescotti, C., Serpilli, F., Lori, V., Nataletti, P., Annesi, D., Moschetto, A., Baruffa, R., De Napoli, G., D'Angelo, F., Di Filippo, S., 2020. Towards more reliable measurements of sound absorption coefficient in reverberation rooms: an Inter-Laboratory Test. Appl. Acoust. 165, 107298. https://doi.org/10.1016/j.apacoust.2020.107298.

Shtrepi, L., Prato, A., 2020. Towards a sustainable approach for sound absorption assessment of building materials: Validation of small-scale reverberation room measurements. Appl. Acoust. 165, 107304 https://doi.org/10.1016/j.apacoust.2020.107304.

Taban, E., Tajpoor, A., Faridan, M., Samaei, S.E., Beheshti, M.H., 2019. Acoustic absorption characterization and prediction of natural coir fibers. Acoust Aust. 47 (1), 67–77. https://doi.org/10.1007/s40857-019-00151-8.

Trematerra, A., Lombardi, I., 2017. Acoustic properties of cork sheets. Key Eng. Mater. 744, 66–70. https://doi.org/10.4028/www.scientific.net/KEM.744.66.

Trevathan, J.W., Pearse, J.R., 2005. The significance of the incident sound field on the sound transmission loss of a finite panel. Build. Acoust. 12 (4), 225–235. https://doi.org/10.1260/135101005775219102.

Yousef, S., Tatariants, M., Tichonovas, M., Kliucininkas, L., Lukošiūtė, S.I., Yan, L., 2020. Sustainable green technology for recovery of cotton fibers and polyester from textile waste. J. Clean. Prod. 254, 120078 https://doi.org/10.1016/j.jclepro.2020.120078.

Zach, J., Korjenic, A., Petranek, V., Hroudov, J., Bednar, T., 2012. Performance evaluation and research of alternative thermal insulations based on sheep wool. Energy Build. 49, 246–253. https://doi.org/10.1016/j.enbuild.2012.02.014.

Zhao, Y., Xu, J., Laurence Davy, J., Liu, Z., Fard, M., 2022. Prediction of random incidence sound absorption coefficients of porous materials. Appl. Acoust. 189, 108625 https://doi.org/10.1016/j.apacoust.2021.108625.